First-in-Human Evaluation of ^{18}F-SynVesT-1, a Radioligand for PET Imaging of Synaptic Vesicle Glycoprotein 2A

Mika Naganawa*, Songye Li*, Nabeel Nabulsi, Shannan Henry, Ming-Qiang Zheng, Richard Pracitto, Zhengxin Cai, Hong Gao, Michael Kapinos, David Labaree, David Matuskey, Yiyun Huang†, and Richard E. Carson†

Yale University PET Center, New Haven, Connecticut

The use of synaptic vesicle glycoprotein 2A radiotracers with PET imaging could provide a way to measure synaptic density quantitatively in living humans. ^{11}C-UCB-J ((*R*)-1-((3-(^{11}C-methyl-^{11}C)pyridin-4-yl) methyl)-4-(3,4,5-trifluorophenyl)pyrrolidin-2-one), previously developed and assessed in nonhuman primates and humans, showed excellent kinetic properties as a PET radioligand. However, it is labeled with the short half-life isotope ^{11}C. We developed a new tracer, an ^{18}F-labeled difluoro-analog of UCB-J (^{18}F-SynVesT-1, also known as ^{18}F-SDM-8), which displayed favorable properties in monkeys. The purpose of this first-in-human study was to assess the kinetic and binding properties of ^{18}F-SynVesT-1 and compare with ^{11}C-UCB-J. **Methods:** Eight healthy volunteers participated in a baseline study of ^{18}F-SynVesT-1. Four of these subjects were also scanned after a blocking dose of the antiepileptic drug levetiracetam (20 mg/kg). Metabolite-corrected arterial input functions were measured. Regional time–activity curves were analyzed using 1-tissue-compartment (1TC) and 2-tissue-compartment (2TC) models and multilinear analysis 1 to compute total distribution volume (V_T) and binding potential (BP_{ND}). The centrum semiovale was used as a reference region. The Lassen plot was applied to compute levetiracetam occupancy and nondisplaceable distribution volume. SUV ratio-1 (SUVR-1) over several time windows was compared with BP_{ND}. **Results:** Regional time–activity curves were fitted better with the 2TC model than the 1TC model, but 2TC V_T estimates were unstable. The 1TC V_T values matched well with those from the 2TC model (excluding the unstable values). Thus, 1TC was judged as the most useful model for quantitative analysis of ^{18}F-SynVesT-1 imaging data. The minimum scan time for stable V_T measurement was 60 min. The rank order of V_T and BP_{ND} was similar between ^{18}F-SynVesT-1 and ^{11}C-UCB-J. Regional V_T was slightly higher for ^{11}C-UCB-J, but BP_{ND} was higher for ^{18}F-SynVesT-1, though these differences were not significant. Levetiracetam reduced the uptake of ^{18}F-SynVesT-1 in all regions and produced occupancy of 85.7%. The SUVR-1 of ^{18}F-SynVesT-1 from 60 to 90 min matched best with 1TC BP_{ND}. **Conclusion:** The novel synaptic vesicle glycoprotein 2A tracer, ^{18}F-SynVesT-1, displays excellent kinetic and in vivo binding properties in humans and holds great potential for the imaging and quantification of synaptic density in neuropsychiatric disorders.

Key Words: PET; SV2A; brain imaging; kinetic modeling; synaptic density

J Nucl Med 2021; 62:561–567
DOI: 10.2967/jnumed.120.249144

Received May 8, 2020; revision accepted Jul. 29, 2020.
For correspondence contact: Mika Naganawa or Yiyun Huang, Yale University, 801 Howard Ave., P.O. Box 208048, New Haven, CT 06520.
E-mail: mika.naganawa@yale.edu, henry.huang@yale.edu
*Contributed equally to this work.
†Contributed equally to this work.
Published online Aug. 28, 2020.

Synaptic vesicle glycoprotein 2A (SV2A) is located in the presynaptic vesicle membrane of virtually all synapses (*1*) and is the target of the anticonvulsant drug levetiracetam (*2*). We previously developed ^{11}C-UCB-J ((*R*)-1-((3-(^{11}C-methyl-^{11}C)pyridin-4-yl) methyl)-4-(3,4,5-trifluorophenyl)pyrrolidin-2-one) as a PET radiotracer, tested it in nonhuman primates and humans, and found it to have excellent imaging properties (*3–5*). SV2A PET could provide a way to measure synaptic density quantitatively in living humans and to track changes in synaptic density with disease. For example, SV2A PET imaging with ^{11}C-UCB-J showed lower hippocampal SV2A specific binding in patients with Alzheimer disease than in cognitively normal subjects (*6*). In major depressive disorder (*7*), the severity of depressive symptoms was inversely correlated with SV2A density. Synaptic changes have also been found in Parkinson disease (*8*) and schizophrenia (*9*).

^{11}C-UCB-J has excellent test–retest reproducibility to measure distribution volume (V_T), with a short scan time (~60 min) (*5*). However, it has a half-life of 20 min, which requires the tracer to be produced on-site. An SV2A radiotracer labeled with ^{18}F for PET imaging is attractive for clinical diagnostic applications. We therefore developed ^{18}F-SynVesT-1 ((*R*)-4-(3-Fluoro-5-(fluoro-^{18}F)phenyl)-1-((3-methylpyridin-4-yl)methyl)pyrrolidin-2-one, the difluoro-analog of UCB-J) and demonstrated its suitability for imaging SV2A in rhesus monkeys. ^{18}F-SynVesT-1 has the same favorable properties as ^{11}C-UCB-J: high brain uptake and good specific binding signals (*10*). The previous identifier for this tracer was ^{18}F-SDM-8, as it was part of a series of ^{18}F-labeled UCB-J analogs developed as synaptic density markers (*10*). This tracer has also been studied elsewhere with the identifier ^{18}F-MNI-1126 (*11*). The new name, ^{18}F-SynVesT-1, was since agreed upon between the groups to eliminate future confusion in the field from use of 2 different names for the same radioligand.

In this study, we evaluated ^{18}F-SynVesT-1 in healthy human volunteers and determined a suitable kinetic model for quantitative analysis of ^{18}F-SynVesT-1 imaging data. A subgroup of volunteers also participated in a baseline and blocking study with levetiracetam using both ^{18}F-SynVesT-1 and ^{11}C-UCB-J for comparison.

MATERIALS AND METHODS

Radiotracer Synthesis

^{18}F-SynVesT-1 and ^{11}C-UCB-J were synthesized as described previously (*3,10*).

Human Subjects

Four healthy volunteers (4 men; 44 ± 13 y old; body mass index, 30 ± 2) completed a baseline study with ^{18}F-SynVesT-1. A second group of healthy volunteers (2 men and 2 women; 38 ± 15 y old; body

mass index, 27 ± 4) were enrolled in a baseline-blocking study of ^{18}F-SynVesT-1 and ^{11}C-UCB-J using levetiracetam as the blocking drug. All subjects were screened with a physical exam, medical history, routine laboratory studies, pregnancy tests (for women), and electrocardiography to assess for eligibility. The institutional review board–approved study was also approved by the Yale–New Haven Hospital Radiation Safety Committee and was performed in accordance with federal guidelines and regulations of the United States for the protection of human research subjects contained in title 45, part 46, of the *Code of Federal Regulations.* All subjects gave written informed consent.

Brain PET Studies

PET Imaging. PET images were acquired using the High Resolution Research Tomograph (Siemens Medical Systems), which acquired 207 slices (1.2-mm slice separation) in list mode for 120 min for ^{18}F-SynVesT-1 and 90 min for ^{11}C-UCB-J. A 6-min transmission scan was conducted for attenuation correction. Dynamic scan data were reconstructed in 27 frames (6 × 30 s, 3 × 1 min, 2 × 2 min, and 16 × 5 min) for ^{11}C-UCB-J, with 6 additional 5-min frames for ^{18}F-SynVesT-1, with corrections for attenuation, normalization, scatter, randoms, and dead time using the motion-compensation ordered-subsets expectation maximization list-mode algorithm for resolution-recovery reconstruction (*12*). Event-by-event motion correction (*13*) based on measurements with the Polaris Vicra sensor (NDI Systems) was included in the reconstruction. Subjects were administered ^{18}F-SynVesT-1 as an intravenous injection over 1 min by an automatic pump (PHD 22/2000; Harvard Apparatus). ^{11}C-UCB-J was administered as a bolus for 2 subjects and as a bolus plus infusion for the other 2 subjects. The blocking scan was conducted 3 h after intravenous administration of levetiracetam (^{18}F-SynVesT-1, 20 mg/kg; ^{11}C-UCB-J, 10 mg/kg [n = 3] and 20 mg/kg [n = 1]).

MRI. Each subject underwent MRI for PET image registration. The MRI sequence was a 3-dimensional magnetization-prepared rapid acquisition with a gradient-echo pulse, using an echo time of 2.78 ms, a repetition time of 2,500 ms, an inversion time of 1,100 ms, and a flip angle of 7° on a 3-T whole-body scanner (Trio; Siemens Medical Systems) with a circularly polarized head coil.

Arterial Input Function Measurement. Discrete blood samples were manually drawn every 10 s from 10 to 90 s; every 15 s from 90 s to 3 min; and then at 3.5, 5, 6.5, 8, 12, 15, 20, 25, 30, 45, 60, 75, and 90 min for both tracers, with 2 additional samples taken at 105 and 120 min for ^{18}F-SynVesT-1. Samples were centrifuged to obtain plasma and then counted with a calibrated well counter.

Radiotracer metabolism was analyzed using plasma samples collected at 3, 8, 15, 30, 60, and 90 min after injection for both tracers, with an additional sample at 120 min for ^{18}F-SynVesT-1. Metabolites were analyzed using the column-switching high-performance liquid chromatography method (*14*) to determine the parent fraction, as previously described (*10*). An ultrafiltration-based method (Centrifree; Millipore) was used to measure the plasma free fraction (*10*).

Image Registration and Regions of Interest. PET images were corrected for motion by frame-by-frame registration to a summed image (0–10 min after injection) using a 6-parameter mutual information algorithm (FLIRT; FSL). The summed PET image was then coregistered to the subject's T1-weighted MR image (6-parameter affine registration), which was subsequently coregistered to the automated anatomic labeling template (*15*) in Montreal Neurologic Institute (*16*) space using a nonlinear transformation (BioImage Suite) (*17*). Using the combined transformations from template-to-PET space, regional tissue time–activity curves were generated in the following regions: amygdala, anterior cingulate cortex, caudate nucleus, cerebellum, frontal cortex, globus pallidus, hippocampus, insular cortex, occipital cortex, parietal cortex, posterior cingulate cortex, putamen, temporal cortex, and thalamus. The region of interest for the centrum semiovale (CS) was designed to minimize the partial-volume effect (*18*).

Quantitative Analysis

For ^{18}F-SynVesT-1, regional total distribution volume (V_T) was computed from the time–activity curves using 1-tissue-compartment (1TC) and 2-tissue-compartment (2TC) models. The relative fit quality of 1TC and 2TC models was compared with the F test. Percentage SE (%SE) was estimated from the theoretic parameter covariance matrix. Multilinear analysis 1 (MA1) (*19*) was also applied to estimate V_T by changing the starting time t^* (from 10 to 60 min with 10-min increments). The choice of best kinetic model for ^{18}F-SynVesT-1 was based on analysis of data from the 8 baseline scans.

For comparison of parametric images to ^{11}C-UCB-J, which used the 1TC model (*5*), parametric V_T images for ^{18}F-SynVesT-1 were also generated with the 1TC model using a basis function method, with k_2 limited to the range of 0.01–1.0 min^{-1} and without postsmoothing. All modeling was performed with in-house programs using IDL, version 8.0 (ITT Visual Information Solutions).

The minimal scan duration for V_T quantification was evaluated by considering shorter datasets (30–120 min in 10-min increments, n = 8) using the selected kinetic model. The percentage differences in V_T derived using data from the shorter intervals and 120 min were calculated. The choice of minimum scan time was based on criteria defined previously (*20*).

The CS region was used as a reference region to compute regional binding potential (BP_{ND}) from V_T. The Lassen plot was used to determine target occupancy by levetiracetam and the nondisplaceable distribution volume (V_{ND}) (*21*). The V_{ND} from gray matter regions was compared with baseline V_T in CS to test the suitability of CS as a reference region.

In addition, a simplified outcome measure, the SUV ratio (SUVR), was evaluated in comparison to BP_{ND}. Static SUVR-1, which would equal BP_{ND} at equilibrium, was computed for 9 time windows of 30-min duration (10–40, 20–50, 30–60, 40–70, 50–80, 60–90, 70–100, 80–110, and 90–120 min) and compared with BP_{ND}, calculated from regional V_T ratio (target/reference) − 1. All outcome measures were computed from regional time–activity curve analysis of baseline scans.

RESULTS

Human Injection and Scan Parameters

The mean administered dose of ^{18}F-SynVesT-1 had an activity of 180 ± 7 MBq (range, 167–186 MBq) and 180 ± 4 MBq (range, 175–185 MBq) for the baseline (n = 8) and blocking (n = 4) scans, respectively. Injection and scan parameters are listed in Table 1.

Safety

No significant clinical changes were observed with the administration of ^{18}F-SynVesT-1 in an injected-mass dose of up to 0.55 μg.

Plasma Analysis

Data from plasma analysis are displayed in Figure 1. At 60 min after radiotracer injection, the fraction of radioactivity corresponding to the parent compound was 26% ± 9% (n = 8, baseline) and 26% ± 9% (n = 4, blocking) for ^{18}F-SynVesT-1 and 23% ± 8% (n = 2, baseline) and 23% ± 10% (n = 2, blocking) for ^{11}C-UCB-J. The plasma free fraction was 0.31 ± 0.01 (n = 8, baseline) and 0.30 ± 0.02 (n = 4, blocking) for ^{18}F-SynVesT-1 and 0.27 ± 0.02 (n = 4, baseline) and 0.28 ± 0.02 (n = 4, blocking) for ^{11}C-UCB-J. The parent fraction at 60 min and free fraction in plasma did not significantly differ between baseline and blocking conditions with ^{18}F-SynVesT-1.

Brain Distribution and Kinetics

Typical time–activity curves and their fitting are shown in Figure 2. High uptake was seen in gray matter regions and low uptake in

TABLE 1
Subject Information and PET Scan Parameters

Parameter	^{18}F-SynVesT-1		^{11}C-UCB-J	
	Baseline (n = 8)	Blocking (n = 4)	Baseline (n = 4)	Blocking (n = 4)
Age (y)	41 ± 13	39 ± 15	38 ± 15*	
Body weight (kg)	87.6 ± 13.9	79.1 ± 13.4	80.0 ± 13.1*	
Injected dose (MBq)	180 ± 7	180 ± 4	548 ± 142	637 ± 99
Molar activity at time of injection (MBq/nmol)	218 ± 89	170 ± 49	136 ± 44	127 ± 53
Injected mass (μg)	0.28 ± 0.10	0.35 ± 0.14	1.67 ± 0.58	2.10 ± 0.54

*Data are for baseline and blocking groups combined.
Data are mean ± SD.

white matter regions. The order of regional uptake levels was similar between ^{18}F-SynVesT-1 and ^{11}C-UCB-J. SUV in brain regions peaked at 5–20 min and 10–25 min after injection for ^{18}F-SynVesT-1 and ^{11}C-UCB-J, respectively.

The 2TC model was favored over the 1TC model by the F test (66% of fits), and the differences were found predominantly in the cerebellum, hippocampus, and neocortical regions. In particular, a moderate lack of fit was seen in the cerebellum with the 1TC model. Although the 2TC fits were excellent, kinetic parameters were not reliably estimated (%SE > 100% in 32% of the fits for k_3 and 77% of the fits for k_4), leading to poor estimation of 2TC V_T in 60% of fits (%SE > 10%). In stable V_T cases (%SE < 10%), the estimated k_4 was not small (~0.02). But, in unstable V_T cases (%SE > 100%), the estimated k_4 was very small ($<10^{-9}$). The ratio of k_3/k_4 was also unstable (%SE > 1,000%). Excluding the unreliable 2TC V_T estimates, 1TC V_T values matched exceptionally with those from 2TC (1TC V_T = 1.01 × 2TC V_T – 0.32, R^2 = 1.00). The MA1 method was also tested with a range of t* settings. If t* has a very small effect on V_T, then the 1TC model is appropriate. The results showed that MA1 V_T values derived with different t* settings did not differ from those estimated by 1TC: the percentage differences ranged from 0.2% ± 0.3% (t* = 10 min) to 2.7% ± 0.8% (t* = 60 min). The largest difference was seen in the cerebellum and hippocampus with a t* of 60 min (4%–5%). Given the insensitivity of V_T estimates to t* settings in MA1, the quality of fitting by 1TC, and the excellent match with reliable 2TC V_T, the 1TC model was judged as most appropriate for analysis of ^{18}F-SynVesT-1 imaging data.

The mean 1TC-estimated V_T (mL/cm^3) for ^{18}F-SynVesT-1 ranged from 3.5 ± 0.4 in the CS to 19.3 ± 2.8 in the putamen (Table 2), whereas K_1 estimates (mL/min/cm^3) ranged from 0.112 ± 0.011 (CS) to 0.377 ± 0.040 (putamen). These K_1 values were similar to those of ^{11}C-UCB-J (range, 0.113 ± 0.010 to 0.367 ± 0.047), with a relative difference of 4% ± 8%. The 1TC k_2 estimates (1/min) ranged from 0.014 ± 0.001 (amygdala) to 0.032 ± 0.003 (CS) for ^{18}F-SynVesT-1.

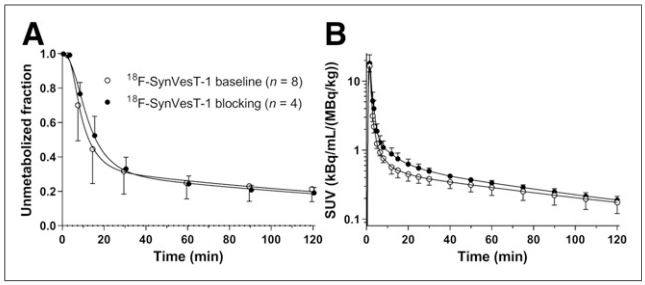

FIGURE 1. Mean ± SD of plasma parent fraction (A) and metabolite-corrected plasma activity (B) in baseline studies and levetiracetam blocking studies with ^{18}F-SynVesT-1.

Voxel-based parametric images were computed with 120 and 90 min of scan data for, respectively, ^{18}F-SynVesT-1 and ^{11}C-UCB-J (Fig. 3). For ^{18}F-SynVesT-1, effectively identical V_T values were obtained with both parametric imaging and time–activity curve fitting: V_T (voxel) = 1.01 × V_T (time–activity curve) + 0.02, R^2 = 1.00.

A minimum scan duration of 60 min was required to satisfy the stability criteria for V_T estimates in all brain regions in 1TC time–activity curve analysis. For specific regions, 60 min was required for the hippocampus and cerebellum, 40 min for the anterior cingulate cortex, and 30 min for other regions (Table 2).

Figure 4 shows examples of Lassen plots using V_T measured with ^{18}F-SynVesT-1 and ^{11}C-UCB-J in the baseline blocking study with levetiracetam (Table 3). The occupancy by a 20 mg/kg dose of levetiracetam was 85.3% ± 4.7% as measured by ^{18}F-SynVesT-1 and 82.5% as measured by ^{11}C-UCB-J, whereas occupancy produced by the 10 mg/kg dose was 76.4% ± 5.6% as measured by ^{11}C-UCB-J. The V_{ND}, determined as the x-intercepts from the Lassen plots, was 2.38 ± 0.33 mL/cm^3 for ^{18}F-SynVesT-1 and 3.13 ± 0.40 mL/cm^3 for ^{11}C-UCB-J. The gray matter V_{ND} was lower than the baseline CS V_T by 32% ± 16% for ^{18}F-SynVesT-1 and 29% ± 13% for ^{11}C-UCB-J; these offsets did not significantly differ between the tracers (P = 0.83). If V_{ND} in CS equals that in gray matter, these data indicate that the BP_{ND} for CS is 0.47 and 0.41 for ^{18}F-SynVesT-1 and ^{11}C-UCB-J, respectively. However, we previously showed that V_{ND} is greater in CS than in gray matter (*18*).

Regional BP_{ND} was compared between the 2 tracers using either baseline CS V_T or Lassen plot V_{ND} as reference values (Supplemental Table 1; supplemental materials are available at http://jnm.snmjournals.org). By either reference method, ^{18}F-SynVesT-1 had higher BP_{ND} than ^{11}C-UCB-J, but the difference was not statistically significant.

Using the CS as a reference region for calculation of BP_{ND} from regional V_T, the mean 1TC BP_{ND} ranged from 2.5 ± 0.5 in the globus pallidus to 4.5 ± 0.5 in the putamen for ^{18}F-SynVesT-1 (Table 2). These values were then compared with SUVRs using different 30-min windows. Percentage differences between SUVR-1 and BP_{ND}

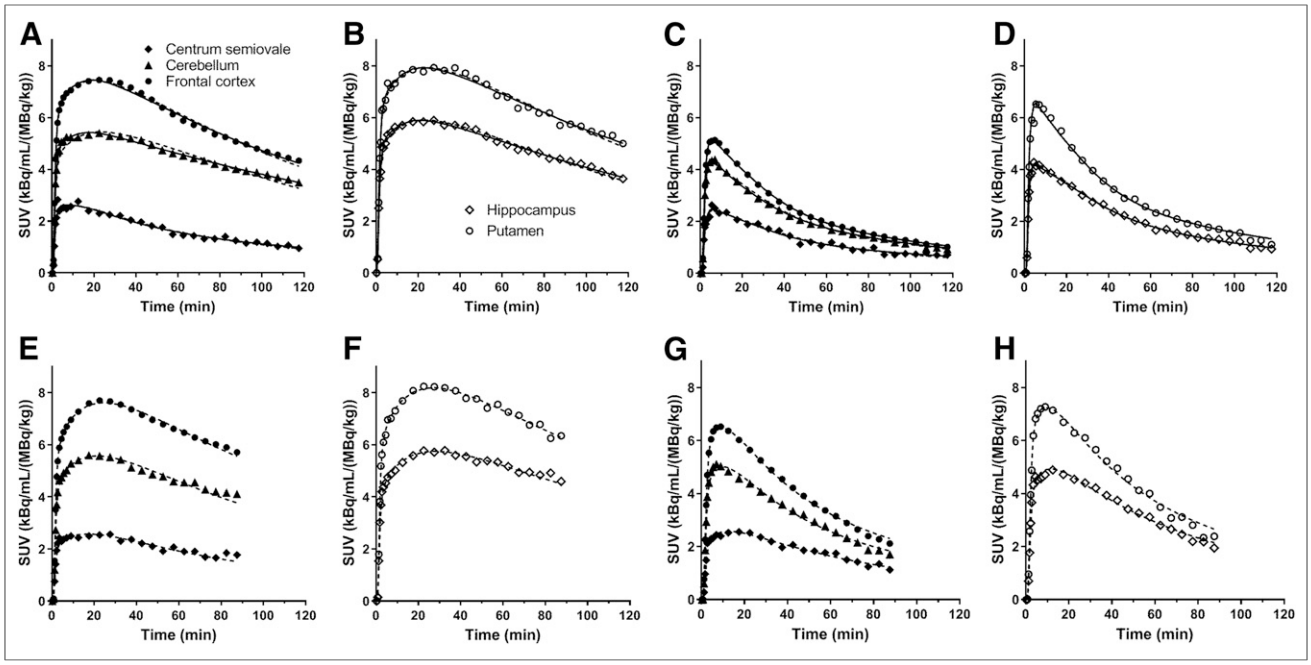

FIGURE 2. Time–activity curves and fittings with 1TC (dotted curve) and 2TC (solid curve) models in same subject under baseline conditions (A and B) and levetiracetam blocking conditions (C and D) with ^{18}F-SynVesT-1, and under same baseline conditions (E and F) and blocking conditions (G and H) with ^{11}C-UCB-J. 2TC model was not applied to ^{11}C-UCB-J.

are shown in Figure 5. The smallest percentage difference was seen when the window for SUVR-1 calculation was 60–90 min. The regression line was as follows: SUVR-1 (60–90 min) = $0.95 \times BP_{ND} + 0.15$ ($R^2 = 0.97$).

DISCUSSION

This first-in-human study of the SV2A PET tracer ^{18}F-SynVesT-1 included baseline PET scans to evaluate methods for kinetic analysis of imaging data, levetiracetam occupancy scans to assess nonspecific binding, and comparison with the established tracer ^{11}C-UCB-J.

In choosing the best kinetic analysis method, we compared the 1TC and 2TC models. The 2TC model was preferred for analysis of ^{18}F-SynVesT-1 imaging data based on the F test in 66% of fits. However, k_3 and k_4 were poorly estimated by the 2TC model, resulting in unreliable V_T estimation. When such unreliable estimates were excluded, the 1TC and 2TC models provided almost

TABLE 2
In Vivo Binding Parameters of ^{18}F-SynVesT-1 and Minimum Scan Time for Stable Measurement, Derived with 1TC Model

Region	V_T (mL/cm^3) (baseline, $n = 8$)	BP_{ND} (baseline, $n = 8$)	Minimum scan time (min)
Putamen	19.3 (14%)	4.5 (11%)	30
Insular cortex	18.8 (16%)	4.3 (13%)	30
Temporal cortex	18.6 (15%)	4.3 (13%)	30
Parietal cortex	17.7 (16%)	4.0 (15%)	30
Amygdala	17.6 (11%)	4.0 (12%)	30
Occipital cortex	17.4 (18%)	3.9 (17%)	30
Anterior cingulate cortex	17.2 (15%)	3.9 (13%)	40
Frontal cortex	16.9 (15%)	3.8 (12%)	30
Caudate nucleus	15.3 (15%)	3.3 (12%)	30
Posterior cingulate cortex	14.2 (27%)	3.0 (29%)	30
Thalamus	13.5 (12%)	2.8 (12%)	30
Cerebellum	13.0 (12%)	2.7 (15%)	60
Hippocampus	13.0 (11%)	2.7 (14%)	60
Globus pallidus	12.6 (20%)	2.5 (19%)	30
CS	3.5 (11%)		30

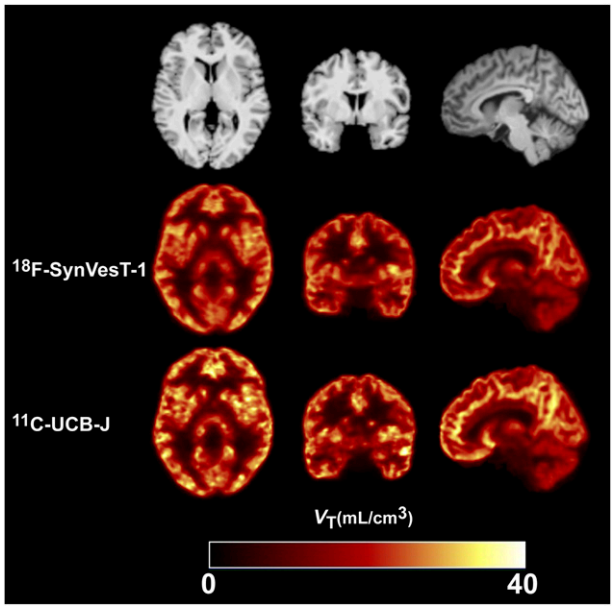

FIGURE 3. MR and coregistered parametric V_T images of ^{18}F-SynVesT-1 (120-min PET data) and ^{11}C-UCB-J (90-min PET data) in same subject, calculated with 1TC model and basis function method.

an identical V_T. Judged from visual inspection of the curve fitting, the 2TC model fitted better in the cerebellum than did the 1TC model, but the fitting results were similar in other regions. Similar results were reported for ^{11}C-UCB-J (*5*); that is, the 2TC model was favored in 73% of fits, and a small lack of fit was seen in the cerebellum and hippocampus.

We then assessed the MA1 method with different t^* settings. For tracers that require the use of the 2TC model (i.e., tracers for which 1TC-derived V_T values differ from those by 2TC), MA1-derived V_T values with early and late t^* settings will be similar to those from the 1TC and 2TC models, respectively. In our study, however, the change in MA1 V_T over different t^* settings was small in all regions, with the largest change being in the cerebellum (4.6%). This observation supports the result that the 1TC and 2TC models provide similar V_T estimates. Given the quality of curve fitting, the small difference in V_T estimated by the 1TC and 2TC models, and the unreliable V_T estimation by 2TC, we chose the 1TC model as best for analysis of ^{18}F-SynVesT-1 imaging data.

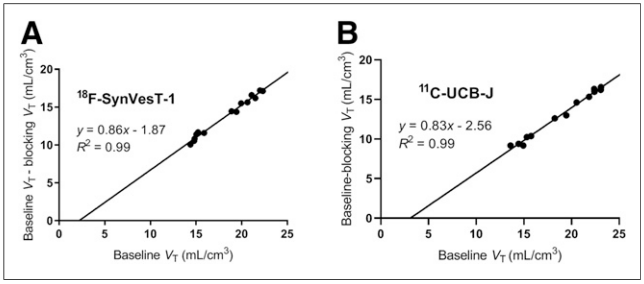

FIGURE 4. Occupancy plots for blocking scans with levetiracetam, 20 mg/kg, measured with ^{18}F-SynVesT-1 (A) and ^{11}C-UCB-J (B) in same subject. Estimated SV2A occupancy values were 86% in A and 83% in B.

Regional V_T values derived from parametric images matched well with those from time–activity curve analysis. Because the statistical quality of V_T images was similarly high for ^{18}F-SynVesT-1 and ^{11}C-UCB-J, no spatial smoothing was required for either tracer. For centers with the ability to produce ^{11}C tracer, ultimately it will be of interest to assess which tracer provides the best image quality with matched radiation dose.

The CS has been proposed as a suitable reference region because of its negligible SV2A level in the baboon brain, as observed by Western blot analysis (*4*). Since CS has been used as a reference region to quantify ^{11}C-UCB-J specific binding (*6,22*), we also evaluated the use of CS as a reference region to compute the BP_{ND} and SUVR of ^{18}F-SynVesT-1. Rossano et al. (*18*) investigated the CS reference region for ^{11}C-UCB-J quantification and optimized the location and size of the region of interest, which were adopted in the current study. As observed previously with ^{11}C-UCB-J, a decrease in ^{18}F-SynVesT-1 V_T was seen in the CS after SV2A blockade with levetiracetam. For both tracers, the V_{ND} determined from the occupancy plot was about 30% lower than the CS V_T. Thus, use of the CS as a reference region might lead to underestimation of BP_{ND} and SUVR. Nonetheless, the CS may still serve as a useful reference region if there is a consistent relationship between CS V_T and V_{ND}, as was shown for ^{11}C-UCB-J (*18*).

Overall, mean V_T was slightly higher for ^{11}C-UCB-J than for ^{18}F-SynVesT-1 across all brain regions, including the CS (Table 3). When the CS was used as a reference region, ^{18}F-SynVesT-1 gave a higher BP_{ND} than did ^{11}C-UCB-J, with the ratio of BP_{ND} (^{11}C-UCB-J)/BP_{ND} (^{18}F-SynVesT-1) being 0.84 ± 0.16 (Supplemental Table 1). When the V_{ND} derived from the Lassen occupancy plots was used, a similar BP_{ND} ratio of 0.79 ± 0.36 was obtained. That is, the mean BP_{ND} of ^{18}F-SynVesT-1 was about 20% higher than that of ^{11}C-UCB-J. Note, however, that with the small size of this study ($n = 4$), these differences were not statistically significant. The lower logD of ^{18}F-SynVesT-1 (2.32 vs. 2.53 for ^{11}C-UCB-J) contributes to a higher free fraction of ligand in the nondisplaceable tissue compartment (f_{ND}) (0.130 vs. 0.086 for ^{11}C-UCB-J) and a lower V_{ND} (2.38 vs. 3.13 for ^{11}C-UCB-J). However, the relative values of BP_{ND} ($=f_{ND}B_{max}/K_D$) also depend on the in vivo K_D. The average in vitro K_i was 3.3 nM for SynVesT-1 and 2.7 nM for UCB-J, taken from 2 sets of measurements published previously (K_i of 2.2 and 4.7 nM, respectively, for SynVesT-1 and 1.5 and 3.0 nM, respectively, for UCB-J) (*23*) and 1 set of our own measurements (K_i of 3.1 nM for SynVesT-1 and 3.7 nM for UCB-J; unpublished data, December 2019) using ^{3}H-UCB-J and human cortex homogenates. Using these in vitro K_i averages as surrogates for in vivo K_D, we found that [f_{ND}/K_D] (^{11}C-UCB-J)/[f_{ND}/K_D] (^{18}F-SynVesT-1) = 0.81, which matches well with the 0.79 found in the present study for BP_{ND} (^{11}C-UCB-J)/BP_{ND} (^{18}F-SynVesT-1).

Another way to compare specific binding between tracers is to use the graphical method of Guo et al. (Guo plot) (*24*), where the sign of the *y*-intercept predicts which tracer has a higher specific binding signal. However, when the Guo plot was applied to compare ^{18}F-SynVesT-1 and ^{11}C-UCB-J, the *y*-intercept could not be reliably estimated because all the data points were far from the origin.

Of the 4 subjects with both ^{11}C-UCB-J and ^{18}F-SynVesT-1 scans, 2 had their ^{11}C-UCB-J scans conducted under a bolus-plus-infusion protocol, and the other 2 received a bolus injection of the radiotracer. This difference in tracer administration methods should not affect the results, since the outcome measure, V_T, was based on kinetic analysis, which accounts for the difference in input function. Although the number of subjects with ^{11}C-UCB-J scans was limited in this

TABLE 3
Total Distribution Volumes Derived with 1TC Model for ^{18}F-SynVesT-1 and ^{11}C-UCB-J Under Baseline and Levetiracetam Blocking Conditions

Region	^{18}F-SynVesT-1 (n = 4)		^{11}C-UCB-J (n = 4)	
	Baseline	Blocking	Baseline	Blocking
Putamen	18.7 (18%)	5.1 (14%)	20.5 (14%)	7.2 (10%)
Insular cortex	18.4 (21%)	4.9 (13%)	19.6 (15%)	6.9 (11%)
Temporal cortex	18.8 (20%)	4.6 (8%)	20.4 (15%)	6.8 (7%)
Parietal cortex	18.1 (21%)	4.3 (6%)	20.1 (15%)	6.6 (7%)
Amygdala	17.4 (13%)	4.7 (12%)	19.1 (13%)	7.0 (13%)
Occipital cortex	17.7 (24%)	4.2 (6%)	19.5 (20%)	6.3 (4%)
Anterior cingulate cortex	17.6 (21%)	4.8 (16%)	19.0 (20%)	7.0 (15%)
Frontal cortex	17.1 (18%)	4.3 (8%)	18.8 (12%)	6.4 (8%)
Caudate nucleus	15.9 (15%)	4.3 (12%)	17.6 (14%)	6.3 (12%)
Posterior cingulate cortex	15.9 (32%)	4.0 (9%)	16.9 (28%)	5.9 (19%)
Thalamus	13.3 (14%)	4.0 (13%)	14.5 (12%)	5.7 (6%)
Cerebellum	13.0 (17%)	3.6 (12%)	13.7 (13%)	5.2 (5%)
Hippocampus	13.2 (13%)	3.8 (11%)	14.1 (10%)	5.5 (10%)
Globus pallidus	11.9 (27%)	4.2 (14%)	12.5 (18%)	5.6 (6%)
CS	3.6 (13%)	2.4 (6%)	4.5 (10%)	3.4 (4%)

Data in parentheses represent %COV (percentage coefficient of variation [intersubject variability]).

study, their regional V_T values were close to those in the literature (*5,18*). For comparison of regional time–activity curves, input functions, and parent fraction curves between tracers, we used the data from the subjects receiving bolus injections of the radiotracers.

To simplify the imaging and analysis protocol for ^{18}F-SynVesT-1, shorter scan times and simplified quantification method are desirable. By comparing V_T values from different scan lengths to those derived from the 120-min scan data, we found that a scan time of 60 min was sufficient to provide stable V_T estimates for ^{18}F-SynVesT-1. For quantification without arterial sampling, we assessed the possibility of using SUVR-1 as a surrogate for BP_{ND}. The SUVR-1 underestimated BP_{ND} at early time windows, and the difference between SUVR-1 and BP_{ND} monotonically increased by shifting the time window. The best match was seen when the time window for SUVR-1 calculation was 60–90 min. Thus, SUVR-1 calculated from 60 to 90 min after injection of ^{18}F-SynVesT-1 can be used as an appropriate substitute for BP_{ND} as a measure of specific binding signal, thus simplifying the imaging and quantification protocols for this SV2A radiotracer. Note, this result was obtained in healthy control baseline scans and could be affected by disease or drug administration. Indeed, SUVR-1 from 60 to 90 min was about 20% lower than BP_{ND} in the levetiracetam blocking scans.

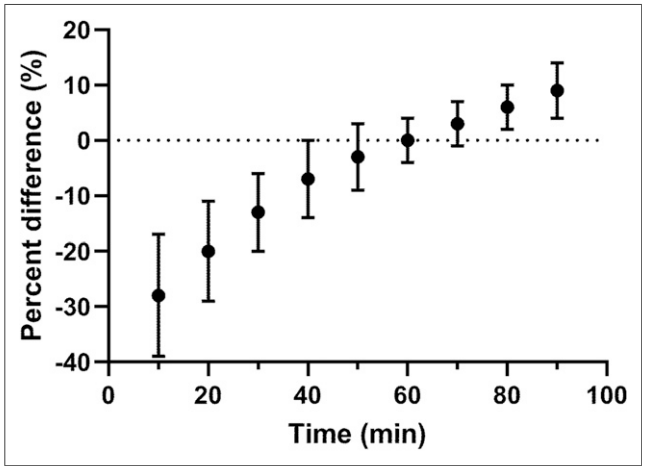

FIGURE 5. Mean and SD of percentage differences between SUVR-1 from different time windows (30-min duration) and 1TC BP_{ND}. Each data point was plotted at beginning of each window for SUVR-1 computation.

CONCLUSION

This study showed that ^{18}F-SynVesT-1 is an excellent PET tracer for SV2A. ^{18}F-SynVesT-1 exhibited properties as good as those of the existing radiotracer ^{11}C-UCB-J: high brain uptake, fast and reversible kinetics, and high specific binding. The 1TC model was chosen as best for quantitative kinetic analysis of ^{18}F-SynVesT-1 imaging data. Regional BP_{ND} levels of ^{18}F-SynVesT-1 were higher than those of ^{11}C-UCB-J. SUVR-1 from 60 to 90 min after injection provided an excellent match with the 1TC BP_{ND} of ^{18}F-SynVesT-1 and thus can serve as a surrogate quantitative measurement of specific binding in a short scan time without invasive arterial sampling. The longer half-life of this tracer will facilitate its broad application in studies of synaptic density in many neurodegenerative and neuropsychiatric populations.

DISCLOSURE

This publication was made possible by CTSA grant UL1 RR024139 jointly from the National Center for Research Resources (NCRR) and the National Center for Advancing Translational Sciences (NCATS),

components of the National Institutes of Health (NIH). The contents of this article are solely the responsibility of the authors and do not necessarily represent the official view of NIH. Financial support was received from R01AG052560, the Michael J. Fox Foundation, and R01AG065474. The radioligand ^{18}F-SynVesT-1 (formerly referred to as ^{18}F-SDM-8) is the subject of international patent application PCT/US2018/018388, "Radiolabeled Pharmaceuticals and Methods of Making and Using Same," filed on February 15, 2018 (inventors: Yiyun Huang, Zhengxin Cai, Songye Li, Nabeel Nabulsi, and Richard E. Carson). No other potential conflict of interest relevant to this article was reported.

ACKNOWLEDGMENT

We appreciate the excellent technical assistance of the staff at the Yale University PET Center.

KEY POINTS

QUESTION: Does ^{18}F-SynVesT-1 show kinetic properties suitable for quantifying SV2A density in humans, in comparison with the existing SV2A tracer, ^{11}C-UCB-J?

PERTINENT FINDINGS: ^{18}F-SynVesT-1 showed excellent in vivo properties, with high brain uptake, reversible kinetics, and high specific binding, similar to ^{11}C-UCB-J.

IMPLICATIONS FOR PATIENT CARE: This longer-half-life tracer will be more useful for clinical studies in terms of allowing off-site production and distribution.

REFERENCES

1. Bajjalieh SM, Frantz GD, Weimann JM, McConnell SK, Scheller RH. Differential expression of synaptic vesicle protein 2 (SV2) isoforms. *J Neurosci.* 1994;14:5223–5235.
2. Lynch BA, Lambeng N, Nocka K, et al. The synaptic vesicle protein SV2A is the binding site for the antiepileptic drug levetiracetam. *Proc Natl Acad Sci USA.* 2004;101:9861–9866.
3. Nabulsi NB, Mercier J, Holden D, et al. Synthesis and preclinical evaluation of ^{11}C-UCB-J as a PET tracer for imaging the synaptic vesicle glycoprotein 2A in the brain. *J Nucl Med.* 2016;57:777–784.
4. Finnema SJ, Nabulsi NB, Eid T, et al. Imaging synaptic density in the living human brain. *Sci Transl Med.* 2016;8:348ra96.
5. Finnema SJ, Nabulsi NB, Mercier J, et al. Kinetic evaluation and test-retest reproducibility of [^{11}C]UCB-J, a novel radioligand for positron emission tomography imaging of synaptic vesicle glycoprotein 2A in humans. *J Cereb Blood Flow Metab.* 2018;38:2041–2052.
6. Chen MK, Mecca AP, Naganawa M, et al. Assessing synaptic density in Alzheimer disease with synaptic vesicle glycoprotein 2A positron emission tomographic imaging. *JAMA Neurol.* 2018;75:1215–1224.
7. Holmes SE, Scheinost D, Finnema SJ, et al. Lower synaptic density is associated with depression severity and network alterations. *Nat Commun.* 2019;10:1529.
8. Matuskey D, Tinaz S, Wilcox KC, et al. Synaptic changes in Parkinson disease assessed with in vivo imaging. *Ann Neurol.* 2020;87:329–338.
9. Onwordi EC, Halff EF, Whitehurst T, et al. Synaptic density marker SV2A is reduced in schizophrenia patients and unaffected by antipsychotics in rats. *Nat Commun.* 2020;11:246.
10. Li S, Cai Z, Wu X, et al. Synthesis and in vivo evaluation of a novel PET radiotracer for imaging of synaptic vesicle glycoprotein 2A (SV2A) in nonhuman primates. *ACS Chem Neurosci.* 2019;10:1544–1554.
11. Constantinescu CC, Tresse C, Zheng M, et al. Development and in vivo preclinical imaging of fluorine-18-labeled synaptic vesicle protein 2A (SV2A) PET tracers. *Mol Imaging Biol.* 2019;21:509–518.
12. Carson RE, Barker WC, Liow JS, Johnson CA. Design of a motion-compensation OSEM list-mode algorithm for resolution-recovery reconstruction for the HRRT. In: *2003 IEEE Nuclear Science Symposium Conference Record.* IEEE; 2003:3281–3285.
13. Jin X, Mulnix T, Gallezot JD, Carson RE. Evaluation of motion correction methods in human brain PET imaging: a simulation study based on human motion data. *Med Phys.* 2013;40:102503.
14. Hilton J, Yokoi F, Dannals RF, Ravert HT, Szabo Z, Wong DF. Column-switching HPLC for the analysis of plasma in PET imaging studies. *Nucl Med Biol.* 2000;27:627–630.
15. Tzourio-Mazoyer N, Landeau B, Papathanassiou D, et al. Automated anatomical labeling of activations in SPM using a macroscopic anatomical parcellation of the MNI MRI single-subject brain. *Neuroimage.* 2002;15:273–289.
16. Holmes CJ, Hoge R, Collins L, Woods R, Toga AW, Evans AC. Enhancement of MR images using registration for signal averaging. *J Comput Assist Tomogr.* 1998;22:324–333.
17. Papademetris X, Jackowski M, Rajeevan N, Constable RT, Staib LH. Bioimage suite: an integrated medical image analysis suite. *Insight J.* 2006;2006:209.
18. Rossano S, Toyonaga T, Finnema SJ, et al. Assessment of a white matter reference region for ^{11}C-UCB-J PET quantification. *J Cereb Blood Flow Metab.* 2020;40:1890–1901.
19. Ichise M, Toyama H, Innis RB, Carson RE. Strategies to improve neuroreceptor parameter estimation by linear regression analysis. *J Cereb Blood Flow Metab.* 2002;22:1271–1281.
20. Frankle WG, Huang Y, Hwang DR, et al. Comparative evaluation of serotonin transporter radioligands ^{11}C-DASB and ^{11}C-McN 5652 in healthy humans. *J Nucl Med.* 2004;45:682–694.
21. Cunningham VJ, Rabiner EA, Slifstein M, Laruelle M, Gunn RN. Measuring drug occupancy in the absence of a reference region: the Lassen plot re-visited. *J Cereb Blood Flow Metab.* 2010;30:46–50.
22. Koole M, van Aalst J, Devrome M, et al. Quantifying SV2A density and drug occupancy in the human brain using [^{11}C]UCB-J PET imaging and subcortical white matter as reference tissue. *Eur J Nucl Med Mol Imaging.* 2019;46:396–406.
23. Patel S, Knight A, Krause S, et al. Preclinical in vitro and in vivo characterization of synaptic vesicle 2A-targeting compounds amenable to F-18 labeling as potential PET radioligands for imaging of synapse integrity. *Mol Imaging Biol.* 2020;22:832–841.
24. Guo Q, Owen DR, Rabiner EA, Turkheimer FE, Gunn RN. A graphical method to compare the in vivo binding potential of PET radioligands in the absence of a reference region: application to [^{11}C]PBR28 and [^{18}F]PBR111 for TSPO imaging. *J Cereb Blood Flow Metab.* 2014;34:1162–1168.